

Three-dimensional adaptive neural network guidance law against maneuvering targets

Si Yujie^{1*}, Xiong Hua¹, Xiong Shaofeng¹

¹ Beijing Institute of Electronic System Engineering, 100854, People's Republic of China

Corresponding author: Si Yujie, Engineer, email: siyujiehit@126.com,
Cel. 16619893261

Abstract: In the modern warfare, missiles are required to attack maneuvering targets. However, saturation is a potential problem for actuators of guidance systems to be considered. This paper concentrates on the problem of designing a three-dimensional nonlinear guidance law accounting for saturation nonlinearity. To solve the physical constraints of missile actuators, an anti-disturbance and anti-saturation terminal sliding mode guidance law is provided based on radial basis functions neural networks. Numerical simulations are introduced to demonstrate the effectiveness and superiority of the designed composite guidance law in theory.

Keywords: Sliding mode control; Impact angle; Anti-saturation guidance law; Neural network method; Hyperbolic tangent function

1. Introduction

With the rapid development of the aerospace weapon industry, air defense systems are drawing more and more attentions. Because attacking the target with a specific impact angle can improve the lethality of warheads, guidance laws with terminal impact angle constraints have become a hot topic recently. Meanwhile, many methods have been proposed in this field such as proportional navigation guidance law (PNGL), the biased pure PNGL (BPPNGL), and optimal control method. In recent decades, the sliding mode control (SMC) theory is proposed, which also provides an effective method for the guidance laws design. A formulation of SMC based PNGL is presented [1]. An adaptive nonlinear guidance law was proposed by using the SMC method so that a missile can accurately intercept a target at the desired impact angle [2]. However, one disadvantage of the traditional sliding mode method is that it can only guarantee the asymptotic convergence of system states.

The engagement scenarios of a missile intercepting targets are three-dimensional scenarios, actually. A three-dimensional fast robust integrated control and guidance law design method was proposed against hypersonic vehicles [3]. Based on the back stepping method, a novel three-dimensional integrated guidance and control scheme were proposed against maneuvering targets [4]. A three-dimensional navigation guidance law was proposed against a moving target with the expected impact direction. The performance of the designed guidance law was essentially bounded within a impact time [5]. A nonlinear suboptimal guidance law was presented for an air launched missile intercepting ground targets, which accurately satisfies terminal impact angle constraints in both azimuth and elevation simultaneously [6].

In addition, there is another potential problem for actuators of the missiles. That is nonlinear saturation, which severely limits system performance. Moreover, the anti-saturation methods have also received great attentions. A three-dimensional guidance law with input saturation constraints and autopilot dynamics was proposed combing an adaptation law to estimate the bound of target acceleration [7]. A three-dimensional anti-saturation integrated guidance and control law with impact angle constraints was developed for intercepting a ground fixed target [8]. A hyperbolic

tangent function was employed to approximate the saturation function and the auxiliary system including a Nussbaum function established to compensate for the approximation error [9].

In the actual battlefield, the information of targets including acceleration and angles is difficult to be measured or estimated accurately. Considering all of the above problems, this study is devoted to design a composite guidance law based on the sliding mode control theory. The content of this paper is arranged as follows. In Section 2, three-dimensional engagement dynamics are established. In Section 3, a novel anti-saturation guidance law is designed by using radial basis functions neural networks. In addition, the theoretical analysis of the guidance law is given. Simulations are presented in Section 4. This paper is finished with conclusions in Section 5.

2. Problem statement

Many of the existing literatures usually decouple the three-dimensional guidance model into two two-dimensional orthogonal models, and then design guidance laws. This way is evidently not in conformity with the reality, and even affects the guidance accuracy. In this study, a three-dimensional coupled model is established according to the three-dimensional geometry, and three-dimensional guidance laws will be designed.

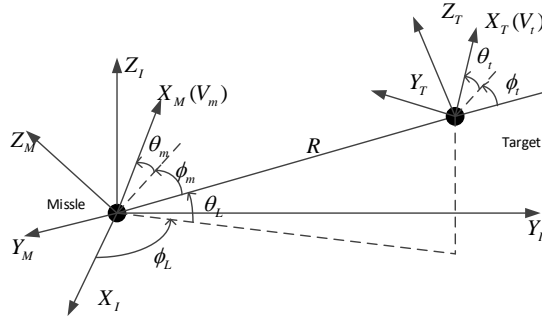


Fig.1. Geometry in three-dimensional space

The three-dimensional guidance geometry of a missile M intercepting a maneuvering target T is presented in Fig.1. $MX_I Y_I Z_I$, $MX_M Y_M Z_M$ and $TX_T Y_T Z_T$ represent the inertial reference frame, missile velocity coordinate system and target velocity coordinate system, respectively. R represents the LOS distance. V_m and V_t are the missile velocity and target velocity, and assumed that the missile and target fly at constant speed in this study. θ_m and ϕ_m are the directions of V_m with respect to the LOS frame. θ_t and ϕ_t are the directions of V_t with respect to the LOS frame. θ_L and ϕ_L are the directions of LOS with respect to the inertial reference frame. a_{ym} and a_{zm} are lateral accelerations of the missile in the yaw and pitch directions. a_{yt} and a_{zt} are target accelerations. Then, the three-dimensional engagement dynamic systems can be expressed as Eqs.(1)-(7) [10].

$$\dot{R} = (\rho \cos \theta_t \cos \phi_t - \cos \theta_m \cos \phi_m) V_m \quad (1)$$

$$R \dot{\theta}_L = (\rho \sin \theta_t - \sin \theta_m) V_m \quad (2)$$

$$\dot{\phi}_L R \cos \theta_L = (\rho \cos \theta_t \sin \phi_t - \cos \theta_m \sin \phi_m) V_m \quad (3)$$

$$\dot{\theta}_m = \frac{a_{zm}}{V_m} - \dot{\phi}_L \sin \theta_L \sin \phi_m - \dot{\theta}_L \sin \theta_m - \dot{\phi}_m \cos \theta_m \quad (4)$$

$$\dot{\phi}_m = \frac{a_{ym}}{V_m \cos \theta_m} + \dot{\phi}_L \sin \theta_L \cos \phi_m \tan \theta_m - \dot{\theta}_L \sin \phi_m \tan \theta_m - \dot{\phi}_L \cos \theta_L \quad (5)$$

$$\dot{\theta}_t = \frac{a_{zt}}{\rho V_m} - \dot{\phi}_L \sin \theta_L \sin \phi - \dot{\theta}_L \cos \phi \quad (6)$$

$$\dot{\phi} = \frac{a_{yt}}{\rho V_m \cos \theta_t} + \dot{\phi}_L \sin \theta_L \cos \phi \tan \theta_t - \dot{\theta}_L \sin \phi \tan \theta_t - \dot{\phi}_L \cos \theta_L \quad (7)$$

where $\rho = \frac{V_t}{V_m}$. To obtain the dynamics of θ_L and ϕ_L , on differentiating Eqs. (2) and (3), the coupled nonlinear second-order dynamics of θ_L and ϕ_L with respect to a_{zm} and a_{ym} can be summarized as

$$\ddot{\theta}_L = \frac{\cos \theta_t}{R} a_{zt} - \frac{\cos \theta_m}{R} a_{zm} - \dot{\phi}_L^2 \cos \theta_L \sin \theta_L - \frac{2\dot{R}\dot{\theta}_L}{R} \quad (8)$$

$$\begin{aligned} \ddot{\phi}_L = & \frac{\cos \phi}{R \cos \theta_L} a_{yt} - \frac{\sin \theta_t \sin \phi}{R \cos \theta_L} a_{zt} + \frac{\sin \theta_m \sin \phi_m}{R \cos \theta_L} a_{zm} \\ & - \frac{\cos \phi_m}{R \cos \theta_L} a_{ym} + 2\dot{\phi}_L \dot{\theta}_L \tan \theta_L - \frac{2\dot{R}\dot{\phi}_L}{R} \end{aligned} \quad (9)$$

Unlike the decoupled engagement dynamics, the dynamics of θ_L and ϕ_L expressed by Eqs. (8) and (9) are systems with nonlinear and strong coupled. Noted that a_{zm} has an effect not only on the elevation direction but also on the azimuth direction. If the guidance laws are designed using the decoupled engagement dynamics, the guidance accuracy might be degraded. In addition, the following assumptions are given about the variables of dynamics (8) and (9).

Assumption 1. Suppose that the target accelerations, a_{yt} and a_{zt} , are bounded and satisfy $|a_{yt}| \leq a_1$, $|a_{zt}| \leq a_2$, for all $t \geq 0$, where a_1 and a_2 are the upper bound of the target accelerations.

Assumption 2. Suppose that the signals R , \dot{R} , θ_L , ϕ_L , $\dot{\theta}_L$, $\dot{\phi}_L$, θ_m , and ϕ_m can be measured. θ_m and ϕ_m satisfy $\theta_m, \phi_m \neq \pm(\pi/2)$.

Assumption 3. Suppose that during the terminal process, the relative velocity between the missile and the target is negative. Besides the missile intercepting target by impact occurs when $R = R_0 \neq 0$, but belongs to the interval $[R_{\min}, R_{\max}] = [0.1, 0.25]m$.

Moreover, to facilitate guidance laws design, the relative dynamics, expressed by Eqs. (8) and (9), can also be represented in a more concise form as Eq. (10).

$$\begin{aligned} \begin{bmatrix} \ddot{\theta}_L \\ \ddot{\phi}_L \end{bmatrix} &= \mathbf{F} + \mathbf{B}\mathbf{u} + \mathbf{D} \quad (10) \\ \mathbf{F} &= \begin{bmatrix} -\dot{\phi}_L^2 \cos \theta_L \sin \theta_L - \frac{2\dot{R}\dot{\theta}_L}{R} \\ 2\dot{\phi}_L \dot{\theta}_L \tan \theta_L - \frac{2\dot{R}\dot{\phi}_L}{R} \end{bmatrix}, \quad \mathbf{D} = \begin{bmatrix} d_1 \\ d_2 \end{bmatrix} = \begin{bmatrix} \frac{\cos \theta_t}{R} a_{zt} \\ \frac{\cos \phi}{R \cos \theta_L} a_{yt} - \frac{\sin \theta_t \sin \phi}{R \cos \theta_L} a_{zt} \end{bmatrix} \\ \mathbf{B} &= \begin{bmatrix} -\frac{\cos \theta_m}{R} & 0 \\ \frac{\sin \theta_m \sin \phi_m}{R \cos \theta_L} & -\frac{\cos \phi_m}{R \cos \theta_L} \end{bmatrix}, \quad \mathbf{u} = \begin{bmatrix} a_{zm} \\ a_{ym} \end{bmatrix} \end{aligned}$$

where τ is the control input, and it is multiplied by the matrix \mathbf{B} . The LOS angles can be controlled only if the matrix \mathbf{B} is nonsingular during the engagement, i.e., $R \neq 0$, and θ_m and ϕ_m satisfy $\theta_m, \phi_m \neq \pm(\pi/2)$. With the Assumptions 2 and 3, \mathbf{u} can be applied to control the system (10). According to Assumption 1, Assumption 2 and Assumption 3, \mathbf{D} is bounded.

The main body of this study is to design a three-dimensional guidance law to ensure the successful interception of a maneuvering target at expect impact angles.

3. Guidance laws design

The guidance dynamics are strongly coupled, time varying, and subject to external disturbances. Besides that, the capacity of dynamic actuators is also limited in practice. Any of these aspects would bring considerable difficulty to the guidance laws design. Therefore, this study is devoted to deal with target maneuvers, control input constraints, and external disturbances simultaneously.

In this study, the dynamic actuators can only provide a limit aerodynamic acceleration against a maneuvering target during terminal phase. To satisfy the control saturation constraints, the control input \mathbf{u} is constructed as

$$\mathbf{u} = \text{sat}(\boldsymbol{\tau}) = \begin{bmatrix} \text{sat}(\tau_1) \\ \text{sat}(\tau_2) \end{bmatrix} \quad (11)$$

$$\text{sat}(\tau_i) = \begin{cases} \tau_m & \tau_m < \tau_i \\ \tau_i & -\tau_m \leq \tau_i \leq \tau_m \\ -\tau_m & \tau_i < -\tau_m \end{cases} \quad (i = 1, 2)$$

where $u_m > 0$ is the magnitede constraint. Defining a new state variable \mathbf{x} as:

$$\mathbf{x} = \begin{bmatrix} x_1 \\ x_2 \end{bmatrix} = \begin{bmatrix} \theta_L - \theta_{L_f} \\ \phi_L - \phi_{L_f} \end{bmatrix}$$

where θ_{L_f} and ϕ_{L_f} are the desired LOS angles, and are assumed as constant in this paper. Then Eq.(10) can be expressed as Eq. (12)

$$\ddot{\mathbf{x}} = \mathbf{F} + \mathbf{B}\mathbf{u} + \mathbf{D} = \mathbf{F} + \mathbf{B}\text{sat}(\boldsymbol{\tau}) + \mathbf{D} \quad (12)$$

$\text{sat}(\bullet)$ is a saturation function. To facilitate the control design, the control input subject to saturation type nonlinearity is approximated by a smooth function defined as

$$\text{sat}(\boldsymbol{\tau}) = g(\boldsymbol{\tau}) = \boldsymbol{\tau} + \Delta\boldsymbol{\tau} \quad (13)$$

$$g(\boldsymbol{\tau}) = u_{\max} \tanh\left(\frac{\boldsymbol{\tau}}{u_{\max}}\right) \quad (14)$$

where, $\tanh\left(\frac{\boldsymbol{\tau}}{u_{\max}}\right) = \begin{bmatrix} \frac{e^{\tau_1/u_{\max}} - e^{-\tau_1/u_{\max}}}{e^{\tau_1/u_{\max}} + e^{-\tau_1/u_{\max}}} & \frac{e^{\tau_2/u_{\max}} - e^{-\tau_2/u_{\max}}}{e^{\tau_2/u_{\max}} + e^{-\tau_2/u_{\max}}} \end{bmatrix}^T$. Eq. (14) can be reorganized as

$$\begin{aligned} \ddot{\mathbf{x}} &= \mathbf{F} + \mathbf{B}\mathbf{u} + \mathbf{D} \\ &= \mathbf{F} + \mathbf{B}\text{sat}(\boldsymbol{\tau}) + \mathbf{D} \\ &= \mathbf{F} + \mathbf{B}g(\boldsymbol{\tau}) + \mathbf{D} \\ &= \mathbf{F} + \mathbf{B}\boldsymbol{\tau} + \mathbf{B}\Delta\boldsymbol{\tau} + \mathbf{D} \end{aligned} \quad (15)$$

To nullify the LOS angle errors and the LOS angular rate, an appropriate sliding surface is selected as follows:

$$\mathbf{S} = \begin{bmatrix} s_1 \\ s_2 \end{bmatrix} = \dot{\mathbf{x}} + \alpha\mathbf{x} + \beta f(\mathbf{x}) \quad (16)$$

$$\mathbf{f}(\mathbf{x}) = \begin{bmatrix} f(x_1) \\ f(x_2) \end{bmatrix} \quad (17)$$

$$f(x_i) = \begin{cases} r_1 x_i + r_2 x_i^2 \text{sign}(x_i) & |x_i| < \eta \\ |x_i|^r \text{sign}(x_i) & \text{otherwise} \end{cases} \quad i = 1, 2 \quad (18)$$

$$r_i = (2 - r)\eta^{r-1} \quad (19)$$

$$r_2 = (r-1)\eta^{r-2} \quad (20)$$

where $0 < r < 1$; η , α , and β are positive constants.

The derivative of S can be expressed as Eq. (21).

$$\begin{aligned} \dot{S} &= \ddot{x} + \alpha \dot{x} + \beta \dot{f}(x) \\ &= F + B\tau + B\Delta\tau + D + G \end{aligned} \quad (21)$$

where

$$G = \alpha \begin{bmatrix} \dot{\theta}_L \\ \dot{\phi}_L \end{bmatrix} + \beta \dot{f}(x) \quad (22)$$

$$\dot{f}(x) = \begin{bmatrix} \dot{f}(x_1) \\ \dot{f}(x_2) \end{bmatrix} \quad (23)$$

$$\dot{f}(x_i) = \begin{cases} r_1 \dot{x}_i + 2r_2 x_i \dot{x}_i \text{sign}(x_i) & |x_i| < \eta \\ r |x_i|^{r-1} \dot{x}_i & \text{otherwise} \end{cases} \quad i = 1, 2 \quad (24)$$

Because $B\Delta\tau$ is a continuous function, radial basis functions neural networks can be used to approximate the continuous function.

$$B\Delta\tau = \hat{f}(\bar{x}, \theta^*) + \varepsilon = \theta^{*T} \varphi(\bar{x}) + \varepsilon \quad (25)$$

where, l is called the neural network node number, and

$$\begin{aligned} \bar{x} &= [\theta_L \quad \phi_L \quad \theta_m \quad \phi_m]^T \\ \varphi(\bar{x}) &= [\phi_1(\bar{x}), \phi_2(\bar{x}), \dots, \phi_l(\bar{x})]^T \in \mathbf{R}^l \\ \phi_i(\bar{x}) &= e^{(-\|\bar{x} - c_i\|^2 / \sigma_i^2)}, c_i \in \mathbf{R}^4, i = 1, 2, \dots, l \\ \theta^* &= [\theta_1^*, \theta_2^*], \theta_1^*, \theta_2^* \in \mathbf{R}^l \\ \varepsilon &= [\varepsilon_1, \varepsilon_2]^T \end{aligned}$$

Then,

$$\begin{aligned} \dot{S} &= F + B\tau + B\Delta\tau + D \\ &= F + B\tau + \theta^{*T} \varphi(\bar{x}) + \varepsilon + D \end{aligned} \quad (26)$$

Assumption 4: According to universal approximation property of RBF networks, the maximum mean square value of the approximation error vectors can be written as

$$\|\varepsilon\| \leq \varepsilon_0$$

where ε_0 is a small constant

Assumption 5: The ideal neural networks weights θ_M are bounded so that $\|\theta^*\| \leq \theta_M$ with θ_M is a known bound.

The anti-saturation guidance law designed in this part is as Eq. (27). In addition, an adaptive law (6-77) is designed to estimate the upper bound D of the system external disturbance.

$$\tau = -B^{-1}(F + G + k_1 S + \sigma Q \hat{H} + \hat{\theta}^T \varphi(\bar{x})) \quad (27)$$

$$\dot{\hat{\theta}} = k_2 (\varphi(\bar{x}) S^T - k \hat{\theta}) \quad (28)$$

$$\dot{\hat{H}} = \sigma Q S - \gamma \hat{H} \quad (29)$$

$$\sigma = \begin{bmatrix} \sigma_1 & 0 \\ 0 & \sigma_2 \end{bmatrix}, \quad Q = \begin{bmatrix} \text{sign}(s_1) & 0 \\ 0 & \text{sign}(s_2) \end{bmatrix}$$

where, $k_1, k_2 \in \mathbf{R}^2$ are diagonal matrixes, and diagonal elements are greater than zero.

$\sigma_i > n_i, i=1,2$; $k > 0$, $\gamma > 0$, and $k_{\min} = \min\{k_{11}, k_{12}, \dots, k_{1l}\} > \frac{1}{2}$, $\mathbf{H} = \begin{bmatrix} h_1 \\ h_2 \end{bmatrix}$.

Theorem 1. Consider the systems (1)-(7). Suppose that the observation error \mathbf{D} is bounded, and $\|\mathbf{e}_1\| \leq m$. If choose Eq. (16) as the sliding mode surface, and Eq. (27) as the guidance law, then the state of the system is uniformly ultimately bounded.

Proof: Assuming that $|d_1| \leq h_1$ and $|d_2| \leq h_2$. And $\tilde{\boldsymbol{\theta}} = \boldsymbol{\theta}^* - \hat{\boldsymbol{\theta}}$, $\tilde{\mathbf{H}} = \mathbf{H} - \hat{\mathbf{H}}$. Consider a Lyapunov function candidate as Eq. (30):

$$V = \frac{1}{2} \mathbf{S}^T \mathbf{S} + \frac{1}{2} \tilde{\boldsymbol{\theta}}^T \mathbf{k}_2^{-1} \tilde{\boldsymbol{\theta}} + \frac{1}{2} \tilde{\mathbf{H}}^T \tilde{\mathbf{H}} \quad (30)$$

The time derivative of V results in

$$\begin{aligned} \dot{V} &= \mathbf{S}^T \dot{\mathbf{S}} + \tilde{\boldsymbol{\theta}}^T \mathbf{k}_2^{-1} \dot{\tilde{\boldsymbol{\theta}}} + \tilde{\mathbf{H}}^T \dot{\tilde{\mathbf{H}}} \\ &= \mathbf{S}^T (\mathbf{F} + \mathbf{B}\boldsymbol{\tau} + \boldsymbol{\theta}^{*T} \boldsymbol{\varphi}(\bar{\mathbf{x}}) + \boldsymbol{\varepsilon} + \mathbf{D}) - \tilde{\boldsymbol{\theta}}^T \mathbf{k}_2^{-1} (\mathbf{k}_2 (\boldsymbol{\varphi}(\bar{\mathbf{x}}) \mathbf{S}^T - k\hat{\boldsymbol{\theta}})) + \tilde{\mathbf{H}}^T \dot{\tilde{\mathbf{H}}} \\ &= \mathbf{S}^T (-\mathbf{k}_1 \mathbf{S} - \boldsymbol{\sigma} \mathbf{Q} \hat{\mathbf{H}} + \boldsymbol{\theta}^{*T} \boldsymbol{\varphi}(\bar{\mathbf{x}}) - \hat{\boldsymbol{\theta}}^T \boldsymbol{\varphi}(\bar{\mathbf{x}}) + \boldsymbol{\varepsilon} + \mathbf{D}) - \tilde{\boldsymbol{\theta}}^T \mathbf{k}_2^{-1} (\mathbf{k}_2 (\boldsymbol{\varphi}(\bar{\mathbf{x}}) \mathbf{S}^T - k\hat{\boldsymbol{\theta}})) \\ &\quad + \tilde{\mathbf{H}}^T \dot{\tilde{\mathbf{H}}} \\ &= \mathbf{S}^T (-\mathbf{k}_1 \mathbf{S} - \boldsymbol{\sigma} \mathbf{Q} \hat{\mathbf{H}} + \boldsymbol{\varepsilon} + \mathbf{D} - \tilde{\boldsymbol{\theta}}^T \boldsymbol{\varphi}(\bar{\mathbf{x}})) - \tilde{\boldsymbol{\theta}}^T \mathbf{k}_2^{-1} (\mathbf{k}_2 (\boldsymbol{\varphi}(\bar{\mathbf{x}}) \mathbf{S}^T - k\hat{\boldsymbol{\theta}})) \\ &\quad - \tilde{\mathbf{H}}^T (\boldsymbol{\sigma} \mathbf{Q} \mathbf{S} - \gamma \hat{\mathbf{H}}) \\ &\leq \mathbf{S}^T (-\mathbf{k}_1 \mathbf{S} + \boldsymbol{\varepsilon}) - \mathbf{S}^T \boldsymbol{\sigma} \mathbf{Q} \hat{\mathbf{H}} - \mathbf{S}^T \mathbf{D} + k \tilde{\boldsymbol{\theta}}^T (\boldsymbol{\theta}^* - \tilde{\boldsymbol{\theta}}) - \tilde{\mathbf{H}}^T (\boldsymbol{\sigma} \mathbf{Q} \mathbf{S} - \gamma \hat{\mathbf{H}}) \\ &\leq \mathbf{S}^T (-\mathbf{k}_1 \mathbf{S} + \boldsymbol{\varepsilon}) - \sum_{j=1}^2 \sigma_j \hat{h}_j |s_j| + \sum_{j=1}^2 h_j |s_j| + k \tilde{\boldsymbol{\theta}}^T (\boldsymbol{\theta}^* - \tilde{\boldsymbol{\theta}}) + \sum_{j=1}^2 \sigma_j \hat{h}_j |s_j| \\ &\quad - \sum_{j=1}^2 \sigma_j h_j |s_j| + \gamma \tilde{\mathbf{H}}^T \hat{\mathbf{H}} \\ &\leq \mathbf{S}^T (-\mathbf{k}_1 \mathbf{S} + \boldsymbol{\varepsilon}) + k \tilde{\boldsymbol{\theta}}^T (\boldsymbol{\theta}^* - \tilde{\boldsymbol{\theta}}) - \sum_{j=1}^2 (\sigma_j - 1) h_j |s_j| + \gamma \tilde{\mathbf{H}}^T \hat{\mathbf{H}} \end{aligned} \quad (31)$$

Because

$$\begin{aligned} \tilde{\boldsymbol{\theta}}^T (\boldsymbol{\theta}^* - \tilde{\boldsymbol{\theta}}) &= \tilde{\boldsymbol{\theta}}^T \boldsymbol{\theta}^* - \tilde{\boldsymbol{\theta}}^T \tilde{\boldsymbol{\theta}} \\ &\leq \frac{1}{2} \tilde{\boldsymbol{\theta}}^T \tilde{\boldsymbol{\theta}} + \frac{1}{2} \boldsymbol{\theta}^{*T} \boldsymbol{\theta}^* - \tilde{\boldsymbol{\theta}}^T \tilde{\boldsymbol{\theta}} \\ &= \frac{1}{2} \boldsymbol{\theta}^{*T} \boldsymbol{\theta}^* - \frac{1}{2} \tilde{\boldsymbol{\theta}}^T \tilde{\boldsymbol{\theta}} \end{aligned} \quad (32)$$

and

$$\tilde{\mathbf{H}}^T \hat{\mathbf{H}} = \tilde{\mathbf{H}}^T (\mathbf{H} - \tilde{\mathbf{H}}) \leq \frac{1}{2} \mathbf{H}^T \mathbf{H} - \frac{1}{2} \tilde{\mathbf{H}}^T \tilde{\mathbf{H}} \quad (33)$$

It can be obtained that

$$\begin{aligned} \dot{V} &\leq \mathbf{S}^T (-\mathbf{k}_1 \mathbf{S} + \boldsymbol{\varepsilon}) + k \tilde{\boldsymbol{\theta}}^T (\boldsymbol{\theta}^* - \tilde{\boldsymbol{\theta}}) - \sum_{j=1}^2 (\sigma_j - 1) h_j |s_j| + \gamma \tilde{\mathbf{H}}^T \hat{\mathbf{H}} \\ &\leq \mathbf{S}^T (-\mathbf{k}_1 \mathbf{S} + \boldsymbol{\varepsilon}) + \frac{1}{2} \boldsymbol{\theta}^{*T} \boldsymbol{\theta}^* - \frac{1}{2} \tilde{\boldsymbol{\theta}}^T \tilde{\boldsymbol{\theta}} + \frac{\gamma}{2} \mathbf{H}^T \mathbf{H} - \frac{\gamma}{2} \tilde{\mathbf{H}}^T \tilde{\mathbf{H}} \\ &\leq -\mathbf{k}_1 \mathbf{S}^T \mathbf{S} + \mathbf{S}^T \boldsymbol{\varepsilon} + \frac{1}{2} \boldsymbol{\theta}^{*T} \boldsymbol{\theta}^* - \frac{1}{2} \tilde{\boldsymbol{\theta}}^T \tilde{\boldsymbol{\theta}} + \frac{\gamma}{2} \mathbf{H}^T \mathbf{H} - \frac{\gamma}{2} \tilde{\mathbf{H}}^T \tilde{\mathbf{H}} \\ &\leq -\mathbf{k}_1 \mathbf{S}^T \mathbf{S} + \frac{1}{2} \mathbf{S}^T \mathbf{S} + \frac{1}{2} \|\boldsymbol{\varepsilon}\|^2 + \frac{1}{2} \boldsymbol{\theta}^{*T} \boldsymbol{\theta}^* - \frac{1}{2} \tilde{\boldsymbol{\theta}}^T \tilde{\boldsymbol{\theta}} + \frac{\gamma}{2} \mathbf{H}^T \mathbf{H} - \frac{\gamma}{2} \tilde{\mathbf{H}}^T \tilde{\mathbf{H}} \\ &= -(k_{\min} - \frac{1}{2}) \mathbf{S}^T \mathbf{S} - \frac{1}{2} \tilde{\boldsymbol{\theta}}^T \tilde{\boldsymbol{\theta}} - \frac{\gamma}{2} \tilde{\mathbf{H}}^T \tilde{\mathbf{H}} + \frac{1}{2} \boldsymbol{\theta}^{*T} \boldsymbol{\theta}^* + \frac{\gamma}{2} \mathbf{H}^T \mathbf{H} + \frac{1}{2} \|\boldsymbol{\varepsilon}\|^2 \\ &\leq -\lambda V + \Delta \end{aligned} \quad (34)$$

where

$$\lambda = \lambda_{\min} \left\{ k_{1\min} - \frac{1}{2}, \frac{1}{2}, \frac{\gamma}{2} \right\} \quad (35)$$

$$\frac{1}{2} \theta_{\max} + \frac{\gamma}{2} \mathbf{H}^T \mathbf{H} + \frac{1}{2} \|\boldsymbol{\varepsilon}\|^2 \leq \Delta > 0 \quad (36)$$

Then we can obtain that \mathbf{S} is uniformly ultimately bounded. Referring [11], it is straight forward to show that all the signals in the system are uniformly ultimately bounded. The conclusions of the Theorem have been proved here.

4. Simulation results

In this section, the effectiveness and superiority of the composite guidance law $\boldsymbol{\tau}$ are verified through nonlinear numerical simulations. The set of scene parameters are given as follows.

Table 1 scene parameters

$R(0)$ (m)	1200
$\theta_L(0)$ ($^\circ$)	20
$\phi_L(0)$ ($^\circ$)	60
$\theta_m(0)$ ($^\circ$)	25
$\phi_m(0)$ ($^\circ$)	30
V_m (m/s)	600
$\theta_t(0)$ ($^\circ$)	10
$\phi_t(0)$ ($^\circ$)	160
V_t (m/s)	300
$\theta_f(0)$ ($^\circ$)	25
$\phi_f(0)$ ($^\circ$)	65
a_x (m/s ²)	19.6
a_y (m/s ²)	19.6

The PNGL and nonsingular terminal sliding mode (NTSM) guidance law^[12] were compared to analyze the superiority of the guidance laws proposed in this paper. The PNGL is shown as

$$\mathbf{n}_c = \begin{bmatrix} -N_1 \dot{R} \dot{\theta}_L \\ -N_2 \dot{R} \dot{\phi}_L \end{bmatrix} \quad (37)$$

The NTSM surface is expressed as

$$\boldsymbol{\sigma} = \begin{bmatrix} \sigma_1 \\ \sigma_2 \end{bmatrix} = \mathbf{x} + \frac{1}{\beta} \dot{\mathbf{x}}^{p/q} \quad (38)$$

where $\beta > 0$ is a constant. $p > 0$ and $q > 0$ are odd constants, and satisfy

$$p > q \quad (39)$$

The corresponding NTSMGL is presented as

$$\mathbf{u}_0 = -\mathbf{B}^{-1} \left(\mathbf{N} + \frac{\beta q}{p} \dot{\mathbf{x}}^{2-p/q} + k_0 \boldsymbol{\sigma} + \mathbf{H}_0 \operatorname{sgn}(\boldsymbol{\sigma}) \right) \quad (40)$$

The guidance parameters of \mathbf{u}_0 and PNGL are chosen as $\alpha = 0.5$, $\beta = 2$, $p = 9$, $q = 7$, $k_0 = 0.5$. The parameter in the saturation function is selected as $u_m = 25g$. $k = 0.5$, $\mathbf{k}_1 = \begin{bmatrix} 2 & 0 \\ 0 & 2 \end{bmatrix}$,

$\mathbf{k}_2 = \begin{bmatrix} 12 & 0 \\ 0 & 12 \end{bmatrix}$, $\boldsymbol{\sigma} = \begin{bmatrix} 1.7 & 0 \\ 0 & 1.7 \end{bmatrix}$, $\gamma = 1$ The neural network contains 11 nodes, and the center

vector $\mathbf{c}_i, i=1,2,\dots,l$ is evenly spaced on $[-1,1]\times[-0.01,0.01]$. The radial basis vector $\sigma=1$. The parameters N_1 and N_2 in the PNGL are selected as $N_1=7$ and $N_2=7$.

When the initial scenario is listed in Table 1, the simulation results are shown in Fig. 3. From Fig. 2, it can be observed that all of the three guidance laws can guarantee the successful interception, although the missile under PNGL has a different path with it under τ or \mathbf{u}_0 . Fig. 3 clearly presents that both τ and \mathbf{u}_0 can drive the convergences of θ_L and ϕ_L to the desired values in finite time, but PNGL can not guarantee it. Moreover, τ can guarantee a faster convergence rate than \mathbf{u}_0 . Fig. 4 shows the curves of $\dot{\theta}_L$ and $\dot{\phi}_L$, and it can be clearly observed that the performance of τ in driving the LOS angular rate to zero is superior compared with \mathbf{u}_0 and PNGL. Fig. 5 shows the curves of the missile accelerations. It can be noted that there exists the acceleration saturation phenomenon for τ and \mathbf{u}_0 at the beginning of the guidance process. Additionally, it can be noted that the accelerations of the missile produced by the PNGL are smaller than those under τ or \mathbf{u}_0 . It could all come down to that large accelerations can ensure preferable convergence performances.

Generally, the effectiveness and superiority of τ have been clearly stated.

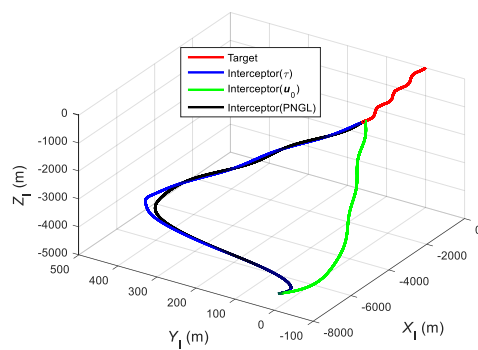


Fig. 2 Relative movement curves

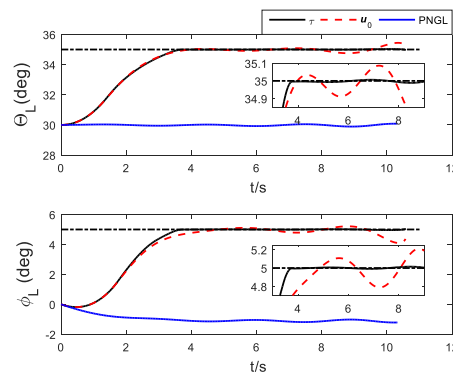


Fig. 3 Curves of θ_L and ϕ_L

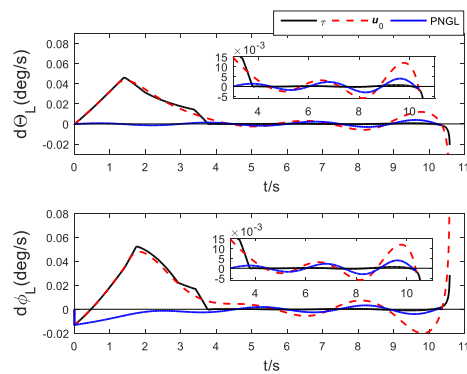


Fig. 4 Curves of $\dot{\theta}_L$ and $\dot{\phi}_L$

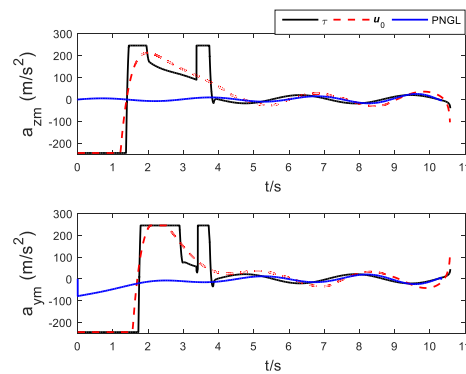


Fig. 5 Missile acceleration profiles

5. Conclusions

A three-dimensional anti-disturbance and anti-saturation terminal sliding mode guidance law has been proposed. Firstly, the three-dimensional coupled guidance dynamics for a missile intercepting a maneuvering target were established. Then, based on the fast nonsingular terminal sliding mode control theory and the radial basis functions neural networks, a novel anti-saturation guidance law was proposed. In addition, the theoretical analysis of guidance laws was also given. Finally, the effectiveness and advantages of the designed guidance laws have been verified by simulations.

References

- [1] Phadke S B, Talole S E. Sliding mode and inertial delay control based missile guidance. *IEEE Transactions on Aerospace and Electronic Systems*, 2012, 48(4): 3331-3346.
- [2] Hou M, Duan G. Integrated guidance and control of homing missiles against ground fixed targets. *Chinese J Aeronaut*, 2008, 21(2): 162-8.
- [3] Song H, Zhang T. Fast robust integrated guidance and control design of interceptors. *IEEE Transactions on Control Systems Technology*, 2016, 24(1): 349-356.
- [4] He S, Wang W, Wang J. Three-dimensional multivariable integrated guidance and control design for maneuvering targets interception. *Journal of the Franklin Institute*, 2016, 353(16): 4330-4350.
- [5] Yoon M G. Relative circular navigation guidance for three-dimensional impact angle control problem. *Journal of Aerospace Engineering*, 2010, 23(4): 300-308.
- [6] Oza H B, Padhi R. Impact-angle-constrained suboptimal model predictive static programming guidance of air-to-ground missiles. *Journal of Guidance, Control, and Dynamics*, 2012, 35(1): 153-164.
- [7] Zhou D, Xu B. Adaptive dynamic surface guidance law with input saturation constraint and autopilot dynamics. *Journal of Guidance, Control, and Dynamics*, 2016: 1155-1162.
- [8] Wang W, Xiong S, Wang S, et al. Three dimensional impact angle constrained integrated guidance and control for missiles with input saturation and actuator failure. *Aerospace Science and Technology*, 2016, 53(2016): 169-187.
- [9] Wang S, Wang W, Xiong S. Impact angle constrained three-dimensional integrated guidance and control for STT missile in the presence of input saturation. *ISA transactions*, 2016, 64(2016): 151-160.
- [10] Song S H, Ha I J. A Lyapunov-like approach to performance analysis of 3-dimensional pure PNG laws. *IEEE Transactions on Aerospace and Electronic Systems*, 1994; 30(1): 238-48.
- [11] Si Y J, Song S M. Three-dimensional Adaptive Finite-time Guidance Law for Intercepting Maneuvering Targets. *Chinese Journal of Aeronautics*, 2017, 30(6): 1985-2003.
- [12] Kumar S R, Ghose D. Three-dimensional impact angle guidance with coupled engagement dynamics. *Proceedings of the Institution of Mechanical Engineers, Part G: Journal of Aerospace Engineering*, 2017, 231(4): 621-641.